Journal of Power Sources 192 (2009) 451–456

Contents lists available at ScienceDirect

Journal of Power Sources

journal homepage: www.elsevier.com/locate/jpowsour

Investigation on the durability of direct methanol fuel cells

Hou-Chin Cha*, Charn-Ying Chen, Jr-Yuan Shiu

Institute of Nuclear Energy Research (INER), 1000, Wenhua Rd., Chiaan Village, P.O. Box 3-14, Lungtan, Taiwan

ARTICLE INFO

Article history:
Received 17 January 2009
Received in revised form 12 March 2009
Accepted 12 March 2009
Available online 24 March 2009

Keywords:
Direct methanol fuel cell (DMFC)
Membrane electrode assembly (MEA)
Durability
Decay rate
Cyclic voltammetry

ABSTRACT

This study addresses the durability of direct methanol fuel cells (DMFCs). Three performance indices including permanent degradation, temporary degradation and voltage fluctuation are proposed to qualify the durability of DMFC. The decay rate, associated with permanent degradation, follows from such failure mechanisms as dissolution, growth and poisoning of the catalyst, while temporary degradation reflects the elimination of the hydrophobic property of the gas diffusion layer (GDL). However, voltage fluctuations reveal different results which cannot stand for degradation phenomenon exactly. In this investigation, such methods of examination as scanning electron microscope (SEM), and X-ray diffraction (XRD) are employed to check the increase in the mean particle size in the anode and cathode catalysts, and the degree is higher in the cathode. The Ru content in the anode catalyst and the specific surface area (SSA) of the anode and cathode catalysts decrease after long-term operation. Moreover, the crossover of Ru from the anode side to the cathode side is revealed by energy dispersive X-ray (EDX) analysis. Electrocatalytic activity towards the methanol oxidation reaction (MOR) at the anode is verified to be weaker after durability test by cyclic voltammetry (CV). Also, the electrochemical areas (ECAs) of the anode and cathode catalysts are evaluated by hydrogen-desorption. SSA loss simply because of agglomeration and growth of the catalyst particles, of course, is lower than ECA loss. The observations will help to elucidate the failure mechanism of membrane electrode assembly (MEA) in durability tests, and thus help to prolong the lifetime of DMFC.

1. Introduction

Direct methanol fuel cells (DMFCs) are attracting increasing attention because of their several advantages such as high power density, ease of fuel storage and refilling, convenience of carrying and mild operating condition. However, DMFC-systems are subject to a tremendous barrier to which in hydrogen-based systems are not: they have a short lifetime, leaving them far from commercialization. Thus, durability testing is of great importance in identifying the mechanism of degradation, and prolonging the lifetime of DMFC by mitigating the detrimental effects of MEA.

The anodic reaction in DMFCs is not ideal because methanol is decomposed into CO, with principal by-products formaldehyde and formic acid, which are aggressive to the MEA. Furthermore, some of these species, strongly adsorbed on the catalyst surface, preventing the adsorption and further reaction of fresh methanol, will facilitate some degradation mechanisms, described below. Like polymer electrolyte membrane fuel cells (PEMFCs), DMFCs have numerous failure mechanisms, including the corrosion of the carbon support [1,2], the sintering and decomposition of catalyst particles [3–7], the poisoning of catalysts by by-products or impurities [8–10], and the variation of hydrophobic/hydrophilic properties in the catalyst and diffusion layers [11,12]. The corrosion of carbon support is referred to the oxidation of carbon, which is often observed in an electrochemical system that will lead to loss of catalysts accompanied with the carbon support. Besides, the change of the microstructures including the sintering and growth of the catalyst particles results in the decrease in the SSA and ECA, and consequently deteriorates the performance of DMFC. Water management is of a great importance to ensure stable operation and high efficiency of DMFC in the long-term test. The loss of hydrophobic property in the catalyst and diffusion layers will make the channels accumulate of too much water which causes reactant starvation, and eventually impacts performance and lifetime of DMFC. DMFCs suffer from two effects—the deactivation of the cathode catalyst by methanol crossover [13,14] and the CO poisoning of the anode catalyst [15,16], which both markedly reduce cell voltage. Methanol crossover through the membrane results in the loss of cathode performance due to the electro-oxidation behaviors of methanol on the cathode, but the situation can be alleviated by coating microporous layer on the gas diffusion layer in order to suppress the undesired fuel. Besides, Pt is the most active metal for the dissociative adsorption of methanol but it is readily poisoned by CO at the anode side, however, Pt–Ru is developed and thus solves the

* Corresponding author.
E-mail address: hccha@iner.gov.tw (H.-C. Cha).

0378-7753/$ – see front matter © 2009 Elsevier B.V. All rights reserved.
doi:10.1016/j.jpowsour.2009.03.028

problem. Therefore, to better understand the failure mechanism in durability testing is the first step in making DMFCs more feasible long-term alternative sources of power.

This work explores the degradation mechanism of cell components during long-term operation. The performance of the as-received MEAs and the test time of 2000 h MEAs are employed to evaluate their health, including permanent degradation, temporary degradation, and voltage fluctuation. Since the degradation mechanism is not the same, the performance indices are proposed to qualify the durability of DMFC due to different MEA processes. To understand the correlation between cell performance and the microstructure of the MEA, electrochemical methods and analytical instruments, such as CV testing, SEM, EDX, XRD are applied.

2. Experimental

2.1. MEA preparation

Two types of MEAs were taken into consideration for DMFC performance test to verify the durability. Sample A was a commercial product with catalyst-coated membrane (CCM), which the anode and cathode catalysts were PtRu (1:1 atomic ratio) and Pt, and the catalyst loading was 2 mg cm^{-2} on each side. The materials using for the GDL on the anode and cathode were carbon paper (SGL) and carbon cloth (BASF), respectively. Sample B was prepared in-house with Nafion® 117 membrane for proton exchange membrane. After Nafion 117 membrane was cleansed by boiling in deionized water, 3 wt.% H_2O_2, 3 wt.% H_2SO_4, deionized water and deionized water again for 1 h in each step, a thin layer of electrode was coated on each surface of the membrane by screen printing with the prepared catalysts. Catalysts of 40 wt.%Pt–20 wt.%Ru (anode) and 60 wt.%Pt (cathode) were supported on a conductive carbon black with a high surface area. The MEA was then obtained by hot pressing at 120 °C and 5–30 kg cm^{-2} for 1–2 min with the same catalyst loading of about 3.5–3.85 mg cm^{-2} in each electrode [17]. The GDL using for sample B was the same with sample A.

2.2. Fabrication and durability test of the MEA

The active area of each MEA was 25 cm^2. The MEA along with the GDL were sandwiched between graphite bipolar plates, and then installed into a pair of titanium-plated current collectors. A serpentine–serpentine flow field was machined into each graphite plate. During the DMFC operation, methanol solution (2.2 wt.%, 20 mL min^{-1}) was supplied to the anode channel at heating temperature of 70 °C while purified air (0.5–1 L min^{-1}) was fed to the cathode channel at room temperature. The long-term durability test was held at constant current mode of 3 A. The cell performance was evaluated by measuring the current–voltage–power characteristics using a test station equipped with a Chroma 63103 electronic load. The test station allowed measurement and recording of voltage, current and temperature.

2.3. Characterization of MEA

After durability test, the MEA was carefully removed from the cell. The CCM was then cut into small pieces, which were used for subsequent SEM, EDX and XRD studies. SEM inspections were performed by a Hitachi S-4800 microscope operating at 15.0 kV, and EDX spectra were acquired by HORIBA EMAX-ENERGY with working distance at 15 mm and acquisition time of 100 s. XRD measurements were carried out on a Bruker D8-Advance X-ray diffractometer using Cu Kα source operated at 40 kV, and tube current maintained at 40 mA. The diffraction peaks 2θ were pursued between 30 and 90° at a scan rate of 3° min^{-1}, with the resolution of 0.05°. CV experiments including activity towards MOR and ECAs of the catalysts were performed by a ZAHNER IM6/6eX system. For activity towards the MOR, the anode was supplied with methanol solution (3 wt.%, 2 mL min^{-1}) at 70 °C while the cathode was fed with high-purity nitrogen (300 mL min^{-1}) at room temperature. For MOR test, Pt on cathode served as dynamic hydrogen electrode (pseudo-DHE), where the protons would be provided by the anode side after the methanol was dissociated. The potential was then scanned from 0.1 to 0.8 V at a scan rate of 20 mV s^{-1}, and the ECAs of the catalysts were evaluated using hydrogen-desorption method. The reaction of interest was the electrochemical reduction of protons (H^+) and subsequent deposition of atomic hydrogen on the surface of the Pt catalyst, $Pt + H^+ + e^- \leftrightarrow Pt–H_{ads}$. The atomic hydrogen adsorption charge density due to this reaction could be determined from the CV scan. The ECA of the Pt catalyst [18] was calculated from the charge density, the well-established quantity for the charge to reduce a monolayer of protons on Pt. For anodic ECA test, the cathode served as dynamic hydrogen electrode (DHE), which was fed with humidified hydrogen at 20 mL min^{-1}. The anode was fed with humidified nitrogen at 300 mL min^{-1}. On the contrary, for cathodic ECA test, the anode served as DHE, which was fed with humidified hydrogen at 20 mL min^{-1}. The cathode was fed with humidified nitrogen at 300 mL min^{-1}. The potential was then scanned from 0 to 0.8 V at a scan rate of 20 mV s^{-1}, both in anode and cathode side.

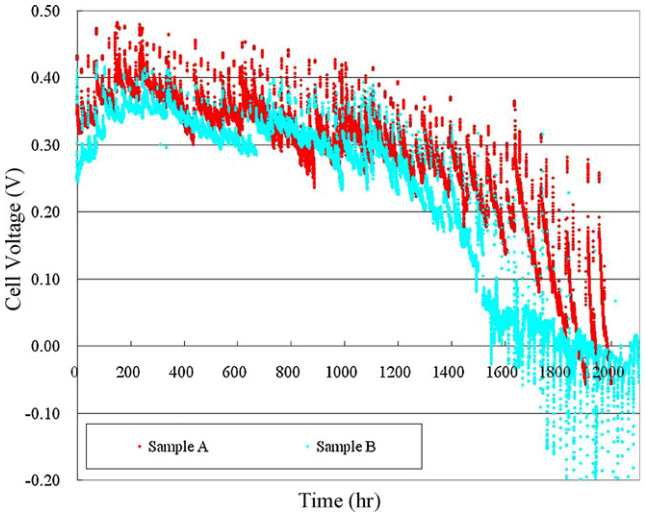

Fig. 1. Durability test of DMFC. Operating condition: cell temperature at 70 °C, 100 mA cm^{-2} (3 A). Anode feed: 2.2 wt.% CH_3OH, flow rate 20 mL min^{-1}. Cathode feed: air, flow rate 0.5–1 L min^{-1}.

3. Results and discussion

3.1. Performance of DMFC

The cell voltage versus operating time during the DMFC 2000 h durability test was shown in Fig. 1. It was observed that voltages of both samples dropped remarkably after operating time of about 1200 h. The cell voltage decreased with time but could be partially recovered after every interruption, which was caused by the stop/restart procedure. The stop/restart procedure maintained the methanol solution circulation, but cut off the air supply without electric load for 1–2 min. Then, turned on the electric load while the air resupplying. As mentioned above, the cell voltage turned back nearly to the last voltage peak due to the stop/restart procedure, but still existed a little bit performance loss that could not be recovered. As shown in Fig. 2, the voltage that could be recovered by the stop/restart procedure was defined to be temporary degradation; on the contrary, the voltage that could not be recovered by the stop/restart procedure was defined to be permanent degradation.

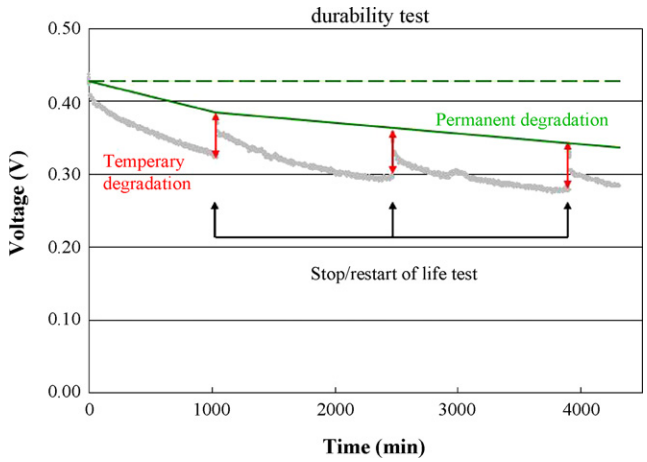

Fig. 2. Illustration of permanent and temporary degradation. Operating condition: cell temperature at 70 °C, 100 mA cm^{-2} (3 A). Anode feed: 2.2 wt.% CH_3OH, flow rate 20 mL min^{-1}. Cathode feed: air, flow rate 0.5–1 L min^{-1}.

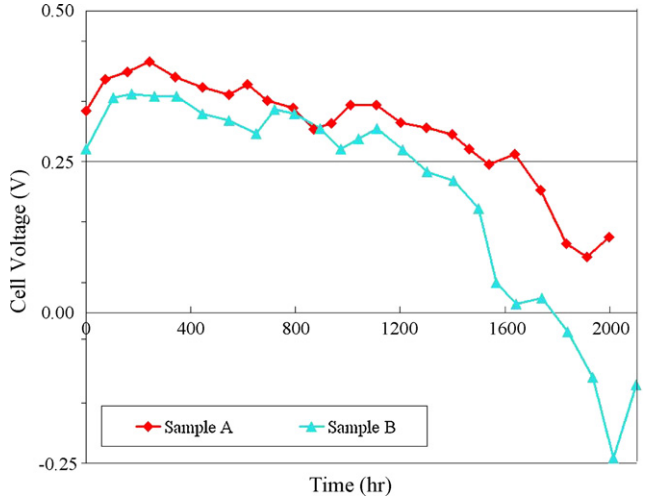

Fig. 3. Average voltages calculated by the mean value during first one thousand minutes over each a hundred hour. Operating condition: cell temperature at 70 °C, 100 mA cm^{-2} (3 A). Anode feed: 2.2 wt.% CH_3OH, flow rate 20 mL min^{-1}. Cathode feed: air, flow rate 0.5–1 L min^{-1}.

The decay rate was used to judge the health of DMFC, and it was usually referred to permanent degradation of the cell voltage. The average voltage shown in Fig. 3 was calculated as a mean value during the first one thousand minutes over each a hundred hour, and the decay rate was evaluated from the average voltage loss over time. The decay rate in each operating period was listed in Table 1. Before operating time of 1200 h, both samples revealed slight and stable degradation, and could be held at about 75% of the maximum average voltage. After that, there was accelerated degradation of sample B, while drastic voltage drop of sample A appeared

Table 1
Decay rate and average voltage of different periods during the durability test.

Operating time (h)	Sample A		Sample B	
	Decay rate (μV h^{-1})	Average voltage (V)	Decay rate (μV h^{-1})	Average voltage (V)
0–1000	72	0.416	75	0.363
1000–1200	145	0.344	90	0.288
1200–1400	100	0.315	255	0.27
1400–1600	250	0.295	850	0.219
1600–1800	210	0.245	125	0.049
1800–2000	555	0.203	660	0.024

Table 2
Temporary voltage loss rate (TVLR) between each stop/restart (S/R) procedure and voltage fluctuation of different operating time during the durability test.

Operating time (h)	Sample A		Sample B	
	TVLR between S/R (mV h^{-1})	Voltage fluctuation (V)	TVLR between S/R (mV h^{-1})	Voltage fluctuation (V)
100	1.717	0.217	1.771	0.093
400	2.161	0.19	1.052	0.1
700	2.26	0.177	0.599	0.081
1000	1.291	0.261	1.573	0.15
1300	2.316	0.183	2.167	0.201
1600	2.791	0.126	3.022	0.416
1900	4.032	0.122	−3.127	0.537

after operating time of 1400 h. A sudden change of the decay rate might imply great degradation of catalysts and polymer electrolyte membrane, and it would significantly affect the lifetime of MEA.

Besides the decay rate, there were some other phenomena that could examine the status of DMFC, such as temporary voltage loss rate between each stop/restart procedure and voltage fluctuation of the cell. Temporary voltage loss rate between each stop/restart procedure, associated with temporary degradation, might exhibit decline in the hydrophobic property of GDL, thus leading to flooding of MEA that would vastly affect subsequent reaction of the catalyst. Voltage fluctuation might indicate that whether reactants were enough, reactants diffused uniformly in time, products could be removed immediately. The above-mentioned situations would go worse whenever a sudden change of decay rate appeared, and the

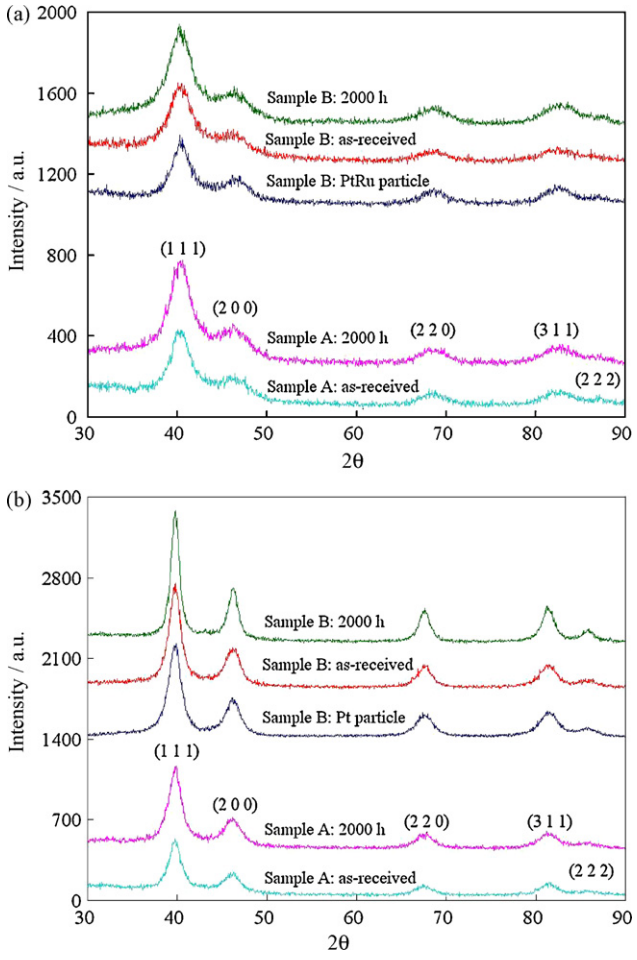

Fig. 4. XRD patterns of the catalysts: (a) anode catalysts and (b) cathode catalysts.

Table 3
Mean particle sizes obtained from XRD.

	Sample A		Sample B	
	Anode (nm)	Cathode (nm)	Anode (nm)	Cathode (nm)
Catalyst particle			3.42	5.21
As-received MEA	3.73	5.07	3.54	5.42
2000 h MEA	4.13	5.86	4.62	7.82

Table 4
Specific surface area of the catalysts.

	Sample A		Sample B	
	Anode ($m^2\ g^{-1}$)	Cathode ($m^2\ g^{-1}$)	Anode ($m^2\ g^{-1}$)	Cathode ($m^2\ g^{-1}$)
Catalyst particle			97.7	53.7
As-received MEA	88.7	55.2	93.9	51.6
2000 h MEA	78.2	47.7	70.2	35.8

historical variations were listed in Table 2. Temporary voltage loss rate between each stop/restart procedure of both samples maintained stable before an operating time of 1300 h, but all accelerated after 1300 h. The negative value of sample B at operating time of 1900 h was an abnormal condition that the cell was initially negative voltage and then crept slowly upwards. It appeared like a severe crossover phenomenon occurred and oxidation was starting to react at the Ru-free electrode (the former cathode electrode). Similarly, voltage fluctuations of both samples did not increase before an operating time of 1300 h, but that of sample B increased severely after 1300 h; that of sample A remained small after 1300 h.

In summary, permanent degradation might exhibit irrecoverable performance loss caused by change of the microstructure such as agglomeration, growth and dissolution of catalysts, and inactivity of active sites due to methanol crossover and CO poisoning after long-term operation. Temporary degradation might display recoverable performance loss caused by elimination of the hydrophobic property of GDL that resulted in flooding of MEA but could be alleviated by changing the air flow rate. Nevertheless, voltage fluctuations of both samples manifested different results that could not stand for degradation phenomenon exactly.

3.2. Structure of catalysts

The XRD patterns of the as-received MEAs with those of the MEAs after 2000 h durability test were shown in Fig. 4. Five characteristic peaks corresponding to Pt (1 1 1), (2 0 0), (2 2 0), (3 1 1) and (2 2 2) were identified from both Pt and PtRu catalysts. These peaks indicated that Pt was present in the face-centered cubic (fcc) structure, and the Pt (1 1 1) peak was selected to calculate the mean particle size of catalyst particle [19].

$$d = \frac{0.9\lambda_{K\alpha 1}}{\beta_{2\theta} \cos \theta_{max}} \quad (1)$$

where d is the mean particle size of catalyst particle, $\lambda_{K\alpha 1}$ the wavelength of X-ray (1.5418 Å), $\beta_{2\theta}$ the width (in rad) of the peak at half-height, and θ_{max} is the angle at the Pt (1 1 1) peak maximum. The mean particle size was then calculated and listed in Table 3. As shown in Table 3, the change of the mean particle size in the anode catalyst varied in the range of 0.4–1.2 nm, while the cathode catalyst in the range of 0.79–2.61 nm. All the mean particle sizes increased after durability test, and the degree was higher in the cathode. It should be noted that, the mean size of PtRu and Pt particles in the powders were almost equivalent to those of the as-received MEA in sample B; therefore, the MEA prepared in-house was reliable so as to represent the unsupported fresh catalyst. The cathode of sample B was selected to verify the variation of catalyst particles by means of SEM. In Fig. 5, the catalysts showed evidently agglomeration and growth that convinced the calculated results in Table 3.

The specific surface area (SSA) of catalyst was calculated from the mean particle size based on XRD through the following formulas, assuming all the particles were in spherical shape [20]:

$$SSA = \frac{6 \times 10^3}{\rho_M \times d} \quad (2)$$

where ρ_M is the density of Pt or PtRu, and d is the mean particle size of catalyst in nm. The ρ_{Pt} is 21.45 g cm^{-3}, and the ρ_{PtRu} value is calculated according to [20]:

$$\rho_{PtRu} = \frac{4 \times 10^{24}(x_{Pt}W_{Pt} + x_{Ru}W_{Ru})}{a_{fcc}^3 \times N_A} \quad (3)$$

where x_{Pt} and x_{Ru} are the atomic fractions in the alloy, W_{Pt} and W_{Ru} the atomic weights, N_A the Avogadro number, and a_{fcc} is the lattice parameter calculated by using the Pt (2 2 0) peak [21]:

$$a_{fcc} = \frac{\sqrt{2}\lambda_{K\alpha 1}}{\sin \theta_{max}} \quad (4)$$

where θ_{max} is the angle at the Pt (2 2 0) peak maximum. The SSA values listed in Table 4 could be obtained through Eqs. (2)–(4). After durability test, the SSA values of sample A decreased 11.8% and 13.6% in the anode and cathode catalysts, respectively, while sample B decreased 25.2% and 30.6%. The cell performance was in relation to the SSA of the catalyst, and it might be the reason that the decay rate of sample B was higher than sample A.

According to the XRD patterns shown in Fig. 4, the angle at the Pt (2 2 0) peak maximum would be shifted due to the Ru content in the anode catalyst. The larger angle value of the Pt (2 2 0) peak

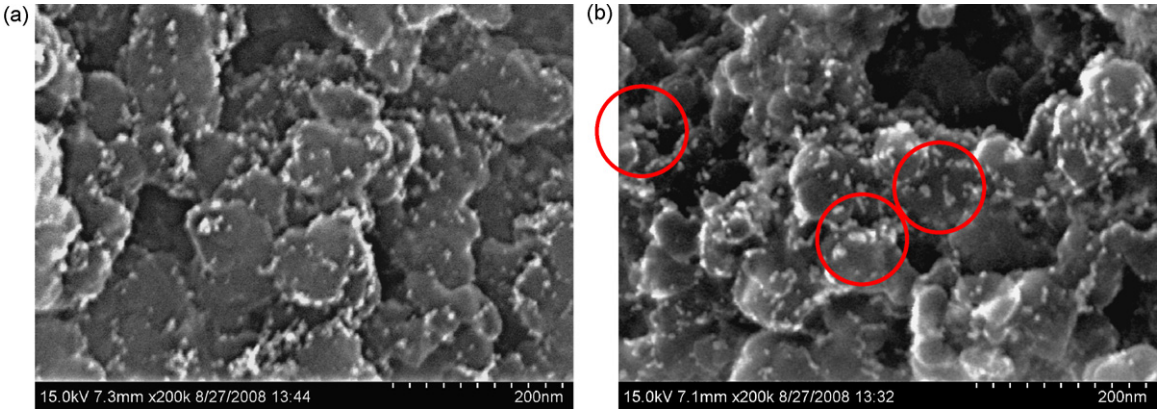

Fig. 5. SEM images of sample B in cathode side: (a) as-received catalyst, (b) catalyst at operating time of 2000 h.

Table 5
Ru atomic ratio in the catalysts.

	Sample A (Ru at.%)	Sample B (Ru at.%)
Catalyst particle		43.19
As-received MEA	41.21	42.2
2000 h	36.25	37.25

maximum, the more Ru atoms were incorporated in the anode catalyst. The Ru atomic fraction in the anode catalyst was calculated by the following equation [21]:

$$a_{fcc} = l_{oc} - kX_{Ru} \quad (5)$$

where l_{oc} (3.906 Å) is the lattice parameter of Pt, k the constant (0.124 Å), and X_{Ru} is the Ru atomic fraction (at.%) presented in anode catalyst. As a result of fact, the Ru atomic fraction in the anode listed in Table 5 decreased with operating time in both samples. The loss parts of Ru atoms were investigated by EDX analysis to see if the Ru penetrated through the membrane from the anode side to the cathode side [21]. EDX spectra shown in Fig. 6 were employed to discover the existence of Ru at the cathode side. Fig. 6(a) and (c) were the as-received MEAs while Fig. 6(b) and (d) were the relative MEAs after durability test. It could be seen that Ru peak appeared after long-term durability test, which implied Ru atoms penetrated through the membrane from the anode side to the cathode side. The crossover of Ru atoms resulted in a lower Ru atomic ratio which listed in Table 5. Besides, parts of Ru atoms might only present as an amorphous oxide, thus could not be detected by XRD. Furthermore, a few Ru atoms associated with Pt–Ru alloys might detach from the carbon support and were flushed out with the methanol solution.

3.3. Cyclic voltammetry

The methanol oxidation current of catalyst shown in Fig. 7 was evaluated by using CV experiment. Samples of the as-received MEAs and with those MEAs after durability test were carried out to examine the activity towards the MOR. The peak voltages of the MOR for sample B before and after durability test were 0.57 and 0.8 V, respectively. The peak voltage of the MOR shifted rightwards or

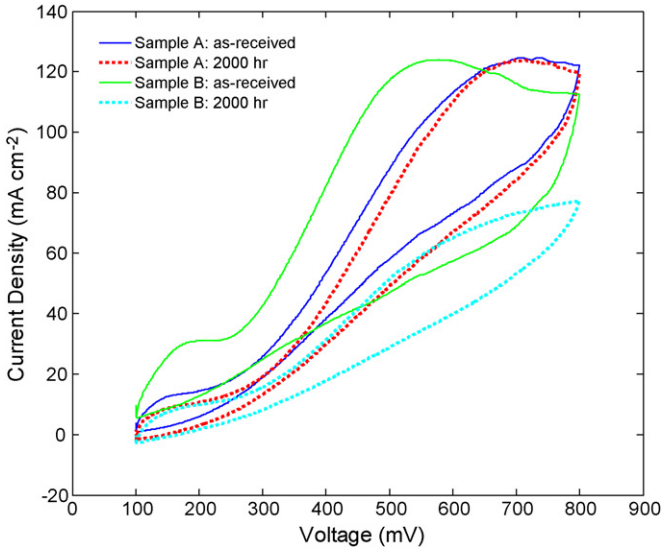

Fig. 7. Electro-catalytic activity towards methanol oxidation reaction (MOR).

even disappeared, which implied that the activity towards the MOR became weaken as higher voltage was needed to make the MOR happen. However, the peak voltage of the MOR for sample A made almost no difference between the as-received MEA and the MEA after durability test. Besides, for example, the MOR current of sample B at 0.5 V dropped obviously from 117 to 52 mA cm^{-2}, while sample A dropped slightly from 89 to 79 mA cm^{-2}. The as-received MEAs yielded higher MOR current than those MEAs after durability test, which exhibited the superior performance of as-received MEAs before durability test. In other words, the activity towards the MOR would reduce after durability test.

Integration of the hydrogen-desorption/adsorption peaks that resulted as a consequence of forward and reverse scans, respectively, could be used to estimate the ECA of catalyst. The CV testing results of hydrogen-desorption method were shown in Fig. 8, and the correlation between the ECA loss and the SSA loss after dura-

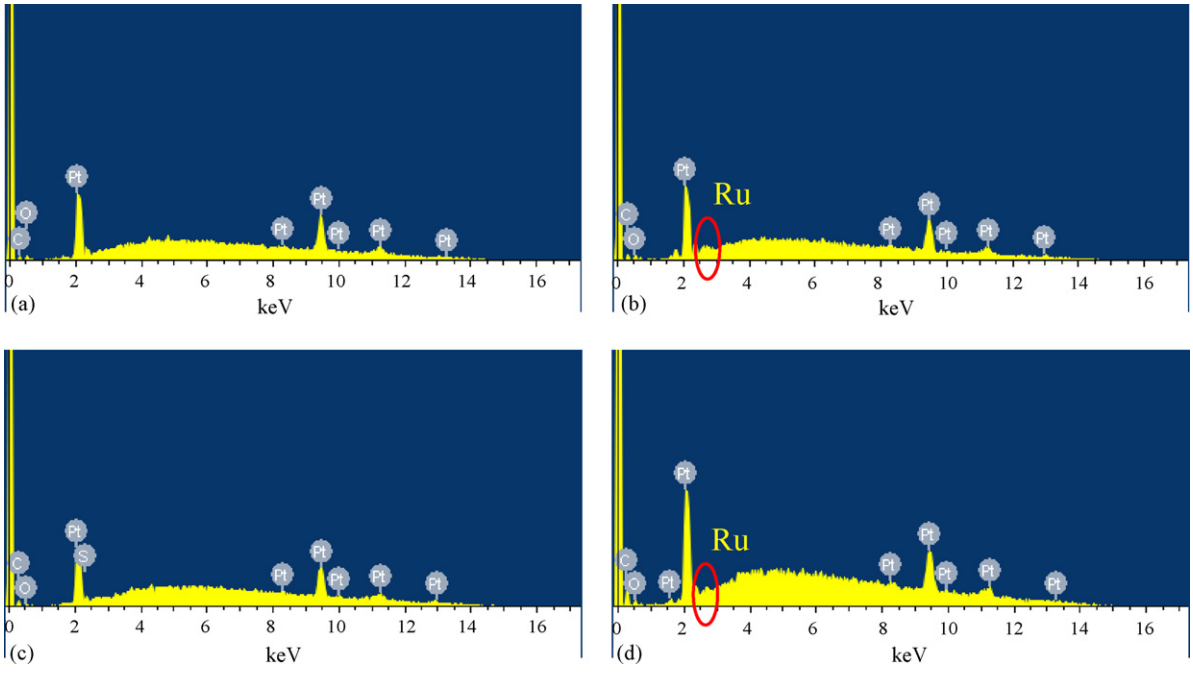

Fig. 6. Representative EDX spectra of cathode catalysts: (a) Sample A: as-received (b) Sample A: 2000 h (c) Sample B: as-received (d) Sample B: 2000 h.

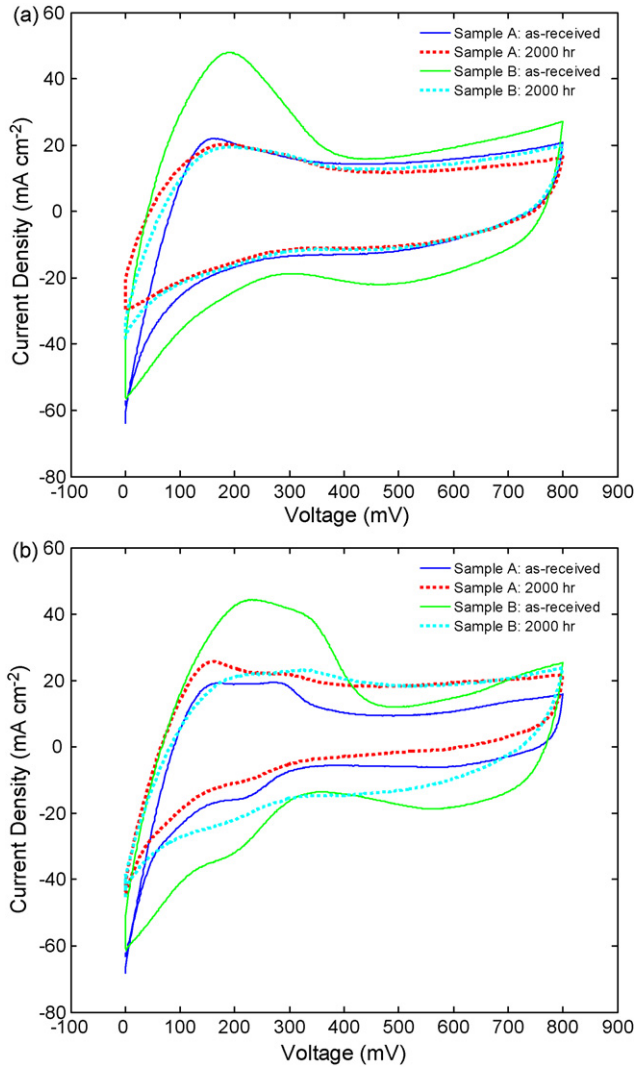

Fig. 8. Electrochemical areas (ECAs) of the catalysts evaluated by hydrogen-desorption test: (a) anode catalysts, (b) cathode catalysts.

Table 6
Comparison of the SSA loss and the ECA loss.

	Sample A		Sample B	
	Anode	Cathode	Anode	Cathode
SSA loss (%)	11.8	13.6	25.2	30.6
ECA loss (%)	19.9	29.0	31.2	36.7

bility test were compared in Table 6. The calculated ECA loss of samples A and B were higher than the SSA loss in both anode and cathode sides. Higher ECA loss might be caused due to the poisoning of catalysts by intermediates and impurities after durability test. The ECA loss estimated the real loss of cell performance other than the SSA loss only represented the change of the microstructure such as agglomeration and growth of catalysts.

4. Conclusion

DMFC durability tests were carried out on both a commercial MEA (sample A) and a MEA constructed in-house (sample B), whose characteristics were examined by XRD, EDX, SEM and CV methods. The proposed performance indices including permanent degradation and temporary degradation could definitely determine whether the MEA was in good health, but voltage fluctuation of the MEA could not stand for degradation phenomenon exactly. According to the decay rate, sample A remained healthy for 1400 h before exhibiting a sudden change of decay rate, while sample B remained healthy for 1200 h. Temporary degradation along with permanent degradation happened almost simultaneously, implying that MEA not only exhibited irrecoverable performance loss caused by change in microstructure and inactivity of the active sites of the catalyst, but also manifested recoverable performance loss due to decline of the hydrophobic property of GDL. The mean particle size of both samples in the anode and cathode catalysts increased during the durability test, and the degree was higher in the cathode. In this study, the Ru atoms in the anode catalyst were discovered to penetrate the membrane from the anode side to the cathode side. The activity towards MOR became weaker along with the ECA of the catalyst became smaller during the durability test as fewer active sites of the catalysts supported to the electrochemical reaction. Higher ECA loss indicated greater worsening of real performance due to poisoning of the catalysts other than SSA loss was caused by microstructural changes due to agglomeration and growth of the catalysts.

References

[1] B.J. Eastwood, P.A. Christensen, R.D. Armstrong, N.R. Bates, J. Solid State Electrochem. 3 (1999) 179.
[2] P.J. Ferreira, G.J. La, O.Y. Shao-Horn, D. Morgan, R. Makharia, S. Kocha, H.A. Gasteiger, J. Electrochem. Soc. 152 (2005) A2256.
[3] Y.Y. Shao, G.P. Yin, J. Zhang, Y.Z. Gao, Electrochem. Acta 51 (2006) 5853.
[4] F. Coloma, A. Sepulveda-Escribano, F. Rodriguez-Reinoso, J. Catal. 154 (1995) 299.
[5] M.S. Wilson, J.A. Valerio, S. Gottesfeld, Electrochem. Acta 40 (1995) 355.
[6] Y.F. Chu, E. Ruckenstein, Surf. Sci. 67 (1977) 517.
[7] J.H. Vleeming, B.F.M. Kuster, G.B. Marin, F. Oudet, P. Courtine, J. Catal. 166 (1997) 148.
[8] U.B. Demirci, J. Power Sources 169 (2007) 239.
[9] E. Antolini, J.R.C. Salgado, E.R. Gonzalez, Appl. Catal. B 63 (2006) 137.
[10] K. Sundmacher, T. Schultz, S. Zhou, K. Schott, M. Ginkel, E.D. Gilles, Chem. Eng. Sci. 5 (2001) 333.
[11] M. Fowler, J.C. Amphlett, R.F. Mann, B.A. Peppley, P.R. Roberge, J. New Mater. Electrochem. Syst. 5 (2002) 255.
[12] W. Schmittinger, A. Vahidi, J. Power Sources 180 (2008) 1.
[13] A. Kuver, W. Vielstich, J. Power Sources 74 (1998) 70.
[14] X. Ren, T.E. Springer, S. Gottesfeld, J. Electrochem. Soc. 147 (2000) 92.
[15] R.A. Lemons, J. Power Sources 29 (1990) 251.
[16] H. Igarashi, T. Fujino, M. Watanabe, J. Electroanal. Chem. 391 (1995) 119.
[17] C.Y. Chen, C.S. Taso, Int. J. Hydrogen Energy 31 (2006) 391.
[18] T.R. Ralph, G.A. Hards, J.E. Keating, S.A. Campbell, D.P. Wilkinson, M. Davis, J. St-Pierre, M.C. Johnson, J. Electrochem. Soc. 144 (1997) 3845.
[19] W. Chen, G. Sun, J. Guo, X. Zhao, S. Yan, J. Tian, S. Tang, Z. Zhou, Q. Xin, Electrochem. Acta 51 (2006) 2391.
[20] A.S. Arico, P.L. Antonucci, E. Modica, V. Baglio, H. Kim, V. Antonucci, Electrochem. Acta 47 (2002) 3723.
[21] J. Prabhuram, T.S. Zhao, Z.X. Liang, R. Chen, Electrochem. Acta 52 (2007) 2649.